

Development of Refractories for Teeming System of Continuous Casting

Kentaro IWAMOTO*
Kazuo ITOH

Toshihiro IMAHASE
Kouichi HAREN

Abstract

Four typical examples of research and development results in the molten steel teeming refractories for the continuous casting system obtained recently in the Krosaki Harima group are introduced. Nozzles (CFN™, CFP™) with an optimized inner bore shape to suppress turbulent flow and minimize the deposition of the inclusions on the nozzle during casting are described with their actual application results. The sliding device, for the sliding nozzle (SN) developed to reduce weight and labor load aiming at future automation (R Series™), is introduced together with the non-impregnated SN plate with low temperature firing (HYPER™). Finally, casting nozzles with improved thermal shock resistance, by bond reformation of the alumina-graphite (AG) system nozzle material focused on low elasticity and high strength (FANON™-TUBE) are explained.

1. Introduction

Continuous casting has quickly expanded in the steel industry since the 1970s, and at present, it is commercially applied to the production of most steel grades with only a few exceptions. The refractories for the teeming system of continuous casting have great influence over the product quality, and there have been many research and development activities to enhance their reliability and functionality. Krosaki Harima Corporation and its group companies have strenuously studied improvement of the quality of the refractory materials for continuous casting, especially those for the teeming system such as the upper nozzles and the submerged entry nozzles (SENs) for tundishes.

Such products of Krosaki Harima include (1) nozzle parts of a new shape, CFN™ and CFP™, designed to suppress turbulence of the steel flow during casting, (2) labor-saving sliding nozzles (SNs), R Series™, for steel ladles developed to decrease the heavy manual labor for changing the hot SN plates soon after casting, (3) low-temperature-fired and no-impregnation SN plates, HYPER™, not containing pitch or tar, and (4) a new type of continuous casting nozzle, FANON™-TUBES, excellent in the thermal shock resistance. The present paper introduces these recently developed refractory products for continuous casting.

2. Clean-flow Nozzle

When Al-killed steel is continuously cast, non-metallic inclusions of alumina systems are often deposited on the inner walls of the upper nozzles and the SENs for the tundish. When this occurs, the effective path sectional area of the teeming system decreases, and when it advances further, the nozzles are clogged, prescribed steel flow into the mold is not maintained, and the casting operation has to be stopped. Moreover, since the inclusion deposits disturb smooth steel flow through the nozzle system, the flow in the mold becomes unstable leading to fluctuation of the steel level and biased flow in the mold, which is likely to cause unstable casting operation and poor quality of the cast products.

There have been many study reports on the alumina deposition in the teeming system. Most refractory engineers have believed that inclusions suspended in molten steel accumulate on and around the nozzle inner surface, new inclusions, which are formed through reactions of the nozzle material and molten steel, also adhere there to increase the alumina deposition, and on this basis, the studies against the deposition have focused on the material quality and the shape of the refractory parts.¹⁾ The following sub-sections report the development of tundish nozzles of a new shape to suppress the turbulence of molten steel flow, minimize the contact of inclusions in steel with the nozzle inner surface, and thus decrease the alumina

* Manager, Flow Control Refractories Division, Krosaki Harima Corporation
1-1 Higashihimamachi, Yahatanishi-ku, Kitakyushu City, Fukuoka Pref. 806-8586

deposition.

2.1 Basic concept of nozzle path shape to suppress steel flow turbulence

The basic concept of the development of a new nozzle path shape is explained below regarding the upper nozzles and the SENs for tundishes. In actual development studies, various adjustments were necessary in consideration of changing operation conditions of the casters. As for such details of the development, the readers are kindly invited to refer to original study reports.^{2,3)}

2.1.1 Upper nozzle for tundish, clean flow nozzle (CFN™)

Figure 1 illustrates the basic concept of the ideal shape of the inner path of the upper nozzle. The flow velocity V of the molten steel in the upper nozzle is determined by converting the potential energy, which is defined by the steel surface level H_r in the tundish, into kinetic energy. By allowing the static pressure of this system to be P , the steel density ρ , and the gravitational acceleration g , Equation (1) (Bernoulli's equation) is obtained according to the law of energy conservation.

$$\rho V^2/2 + \rho g H_r + P = \text{Const.} \quad (1)$$

Then, by allowing Q to be the steel flow amount, V its velocity, and A the inner sectional area of the nozzle path, the following relationship holds true at any vertical position of the nozzle because of the continuity of the fluid.

$$Q = V \cdot A = \text{Const.} \quad (2)$$

Since $A = \pi \cdot R^2$, R being the nozzle inner radius, the relationship between R and the theoretical molten steel head H can be finally expressed as:

$$R \propto H^{-1/4} \quad (3)$$

Formula (3) is the mathematical expression of the ideal curve, which is given on the right-hand side of Fig. 1, of the sectional shape of the nozzle inner path that creates the smallest possible energy loss. In terms of the distribution of the turbulent energy in an upper nozzle calculated by flow analysis, the turbulent energy is clearly far smaller with the new nozzle shape than with the conventional type (see Fig. 2).

2.1.2 Submerged entry nozzle, clean flow port (CFP™)

For the discharge port of a SEN, Equation (1) can be expressed as follows by substituting H with X' , the position in the discharge port in the direction from the outlet to the inlet, and V with V_x , the X component of the steel flow velocity in the port:

$$\rho V_x^2/2 + (\rho g' X' + P + \alpha) = \text{Const.} \quad (4)$$

Here, g' is the gravitational acceleration inside the port, and by allowing the inclination angle of the port with respect to the horizon-

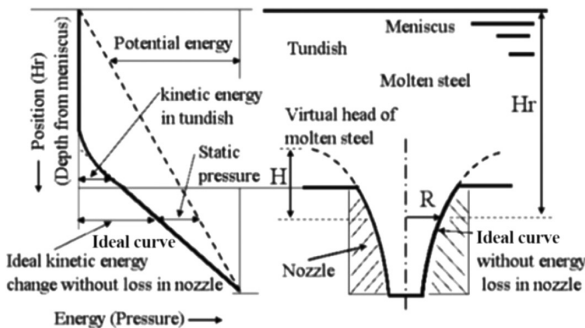


Fig. 1 Conceptual illustration of tundish upper nozzle path shape to suppress turbulent energy (left-hand part: pressure distribution in tundish and upper nozzle, right-hand part: ideal shape of upper nozzle path based on pressure distribution)

tal plane to be θ , it is expressed as $g' = g \times \tan \theta$, and α is the kinetic energy in the discharge port not including the X component but including the energy loss due to turbulence and the like.

Figure 3 schematically illustrates the energy distribution when molten steel flows through the discharge port of a SEN. To obtain a stable energy distribution of the steel flow from the inlet to the outlet of the discharge port, it is necessary to obtain a linear functional kinetic energy with which the second term of Equation (4), namely $(\rho g' X' + P + \alpha)$, which is equal to V_x^2 (kinetic energy), does not have any point of inflection with respect to X' as shown with the non-inflection line in Fig. 3. This means that the following relationship has to be satisfied:

$$V_R^2 \propto R, \quad (5)$$

where, R is the distance in the direction of the steel flow in the discharge port from an imaginary origin assumed to be at its inner end, and V_R the component of the flow velocity (V_x) at position R in the X direction.

On the other hand, the following equation related to the continu-

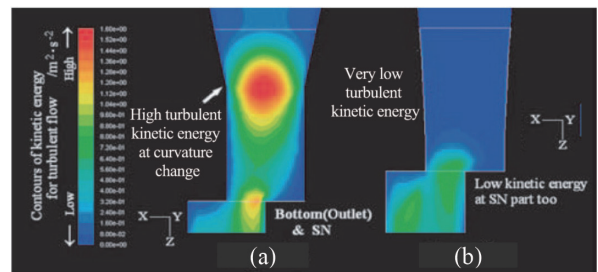


Fig. 2 Calculated turbulent kinetic energy in nozzle path: (a) conventional shape, and (b) ideal shape according to Formula (3)

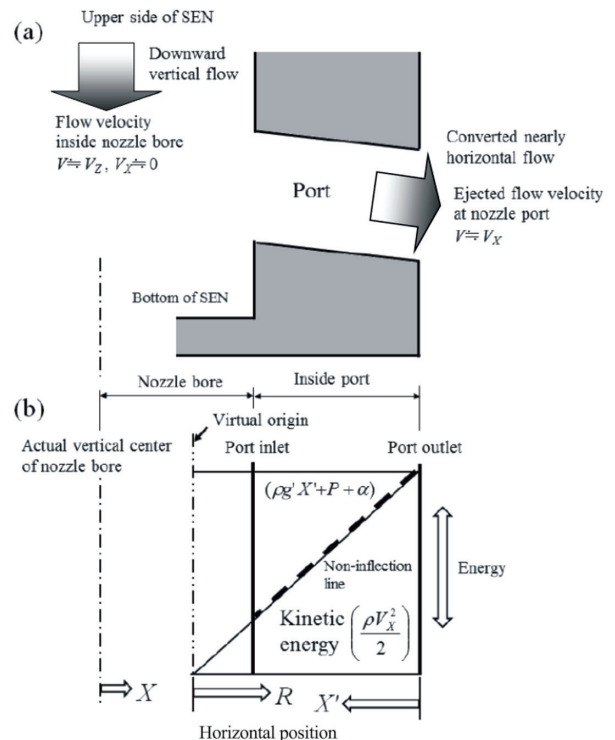


Fig. 3 Flow energy distribution in discharge port of SEN: (a) sectional view of SEN, and (b) flow energy distribution in discharge port

ity of fluid holds true with the steel flowing through the discharge port:

$$Q = V_R \times A_R = Const. \quad (6)$$

Here, A_R is the sectional area of the discharge port at position R . From Equations (5) and (6), the following formula is finally obtained:

$$A_R \propto R^{-1/2} \quad (7)$$

This is the basic formula for designing the shape of a discharge port with which the energy loss and the turbulence of the steel flow are the lowest possible. When a SEN is designed based on this principle, the turbulence inside the discharge port is expected to be minimal, and the steel flow at the outlet of the port is slow and homogeneous.

Figure 4 shows the difference in the velocity vectors of the steel flow at the exit of the discharge port of an optimum shape and the same of a conventional shape obtained by computational fluid dynamics (CFD), and **Fig. 5** compares the two discharge ports in terms of the distribution of turbulent energy in the port. With the conventionally-shaped port, the flow speed is high at the lower region of the exit, and there is a large velocity difference between the upper and the lower regions, but with the newly-shaped port, in contrast, the flow speed distribution is homogeneous. In addition, in terms of the turbulent energy distribution, with the new shape, turbulent energy is lower along the lower port surface than with the conventional shape. This indicates that the newly-shaped port is expected to lower the flow turbulence, minimize the possibility of inclusions in the steel contacting the refractory surface and adhering there, and decrease its corrosion by wear.

2.2 Results of tests in real casting operation

2.2.1 Upper nozzle for tundish

An all-porous, gas-blowing upper nozzle of the conventional shape was fitted at a casting port of a two-strand tundish, another of the new shape to the other port of the same tundish, and the two

specimens were subjected to test casting of six charges; here, the other nozzle parts such as the SNs and the SENs were the same for the two strands. The wear condition of the upper nozzle specimens and skulls on their inner surfaces were examined after the test.

Whereas with the conventionally-shaped specimen, inclusions were found to deposit at the corner where the steel path shape changed, and no such deposition was found with the newly-shaped specimen (see **Fig. 6**). In addition, as seen in **Fig. 7**, whereas there was a layer of inclusion deposit 15 to 20 mm in thickness on the inner wall of the SEN downstream of the conventionally-shaped specimen, there was no such deposit layer on the SEN downstream of that of the new shape. The above seems to indicate that, with the upper nozzle of the developed shape, inclusions did not agglomerate according to fluid analysis, and they were prevented from depositing on the nozzle path surface, and that the bubbles of the gas blowing, together with the developed shape, served effectively to prevent inclusion deposition.

2.2.2 Submerged entry nozzle

A specimen of conventionally-shaped gas-blowing SEN was fitted to a casting port of a two-strand tundish, and another of the developed shape to the other casting port, and after test casting of six charges, the inclusion deposition was examined. With both the specimens, inclusions were found to accumulate at the portion above the discharge ports, but the accumulation tended to be smaller with the newly-shaped specimen (see **Fig. 8**). Fluid analysis predicted that inclusion deposition would be conspicuous at the lower part of the discharge ports, but the result was different presumably because the amount of the gas blown through the nozzle was large, and the steel flow was strongly affected by the upward flow of the gas bubbles.

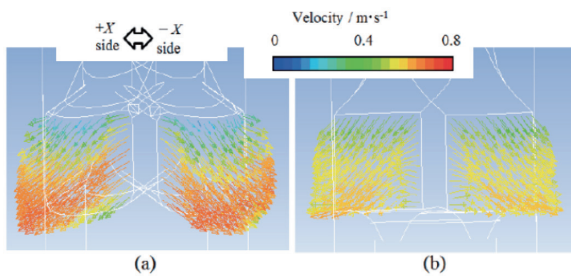


Fig. 4 Three-dimensional distribution of velocity vector in discharge ports of SEN by CFD: (a) conventional shape, and (b) ideal shape

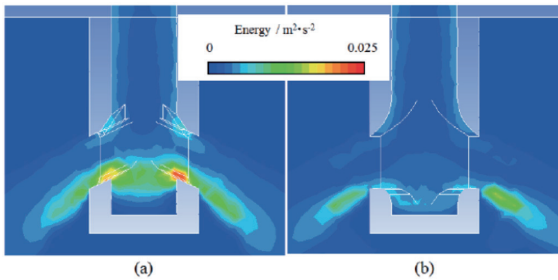


Fig. 5 Two-dimensional distribution of turbulent kinetic energy in SEN and mold in $Y=0$ section by CFD: (a) conventional shape, and (b) ideal shape

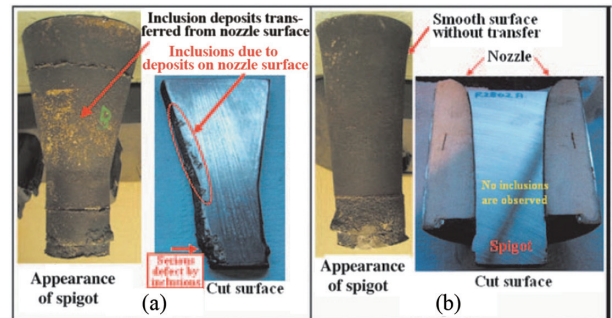


Fig. 6 Comparison of appearances and section surfaces of spigots of upper nozzles of (a) conventional shape and (b) ideal shape

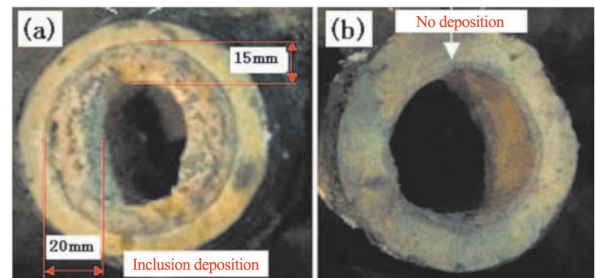


Fig. 7 Cross sections of SENs downstream of upper nozzles of (a) conventional shape and (b) ideal shape

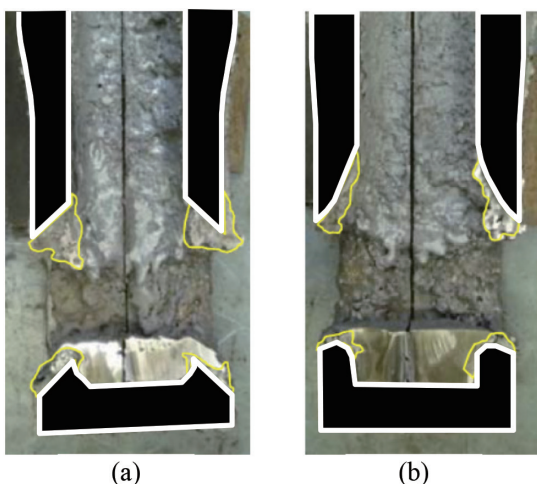


Fig. 8 Cross sections of SENs of (a) conventional shape and (b) ideal shape

3. Labor-saving Sliding Nozzle System for Steel Ladles, R Series™

A sliding nozzle (SN) system is, as shown in Fig. 9, set at the discharge port of a steel ladle or a tundish so as to control the discharge flow of molten steel by changing the opening of the nozzle path: the mechanism consists of two or three refractory plates, each having a nozzle hole, piled to allow reciprocal and linear sliding with respect to each other. Since they are made to slide under a maximum contact pressure of roughly 10 t (all the units herein are metric), they are driven by hydraulic cylinders in most cases. SNs are the most efficient device for controlling the molten steel flow, and as such, they are indispensable for steelmaking and continuous casting processes, where high product quality and productivity are essential.

In usual practice, after casting and deslagging, a SN system of a steel ladle is inspected in terms of the wear of the refractory material, and if judged unsuitable for further use, it is replaced with a new one. Because this SN changing work is physical work that has to be done in a hot condition soon after the end of casting, improvement measures have long been sought. Since the precision of the plate change and loading of the contact pressure are directly linked to the danger of liquid steel leakage, high skill is required to perform the work quickly and accurately.

The newest model of the SN for steel ladles available for commercial use is the R Series™ (R standing for robust, reliable, and rational, see Fig. 10). The refractory parts of the model are designed in tear drop shapes based on FEM analysis. Due to an advanced version of the new quick fit-in plate (NQFP), the simplified mechanism and the compact size, the R Series™ offers improved operability, longer life of the refractory parts, and higher safety.

3.1 Characteristics of R Series™

3.1.1 Structure of metal frames

To reduce the size, the openable metal frame of conventional SNs was divided into two spring boxes arranged on both sides of the sliding parts, and the main frame was divided into a base frame and a slide frame. As a result of extreme weight reduction of the openable part from that of conventional models, the operability has been improved, and the variety and the total number of the component parts have been decreased.

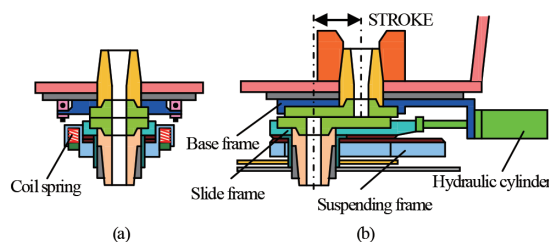


Fig. 9 Sliding nozzle system for steel ladles: (a) side sectional view, and (b) front sectional view

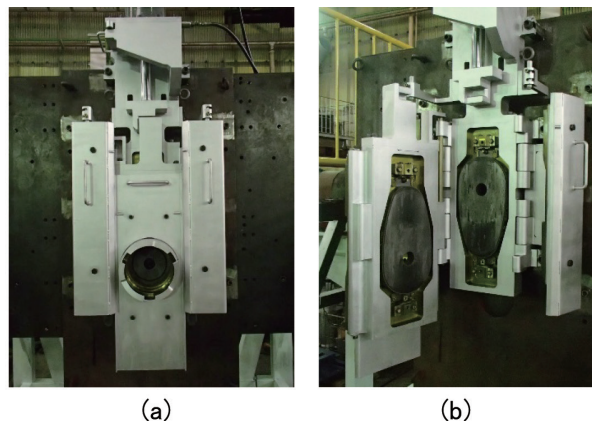


Fig. 10 R Series sliding nozzle system: (a) closed, (b) opened

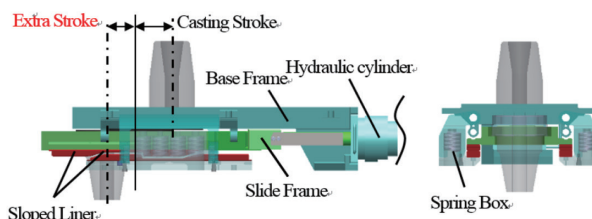


Fig. 11 Conceptual diagram of bearing (contact) pressure loading mechanism

3.1.2 Mechanism for applying contact pressure using sloped liners

As shown in Fig. 11, two metal liners are provided on each side to slide and apply contact pressure to the slide frame and the spring boxes. Each of the liners is sloped at two ends, and when the slide frame moves, the two liners run over each other at each side, and the springs yield by the amount of the run-over. In the ladle preparation area, a hydraulic cylinder having a longer stroke than that for the casting operation is used, and it is possible to apply and release the contact pressure using the extra stroke, without requiring any special handling.

3.1.3 One-action plate fixing mechanism

The advanced NQFP has been introduced to the R Series SN, replacing the conventional method for fixing the SN plate with bolts. A new plate can be fitted into the recess of a SN system in one action using latches and flaps. This mechanism has greatly shortened the work time, eliminated the past problems such as burnt bolts, and secured the plate setting accuracy, which depended on operator skill.

To prevent cracking of the plate, its contour is rounded, and a steel back plate, which has grooves serving as positioning guides and bears the force in the direction of sliding, is welded to the hot

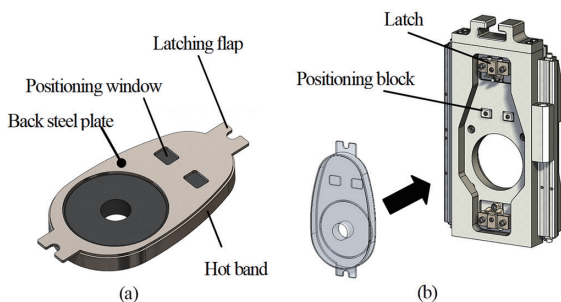


Fig. 12 (a) NQFP unit, (b) fitting into recess of SN system

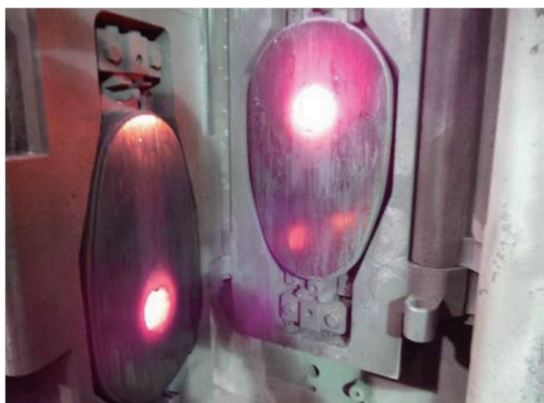


Fig. 13 SN plate opened for NQFP inspection between charges

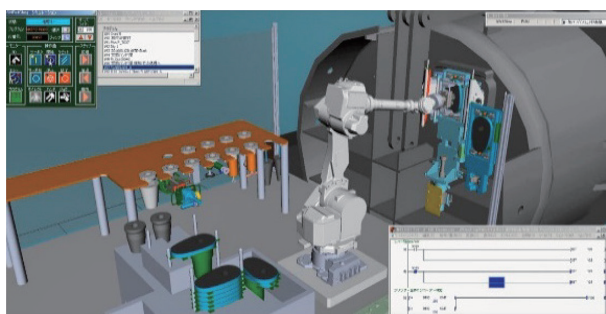


Fig. 14 Automatic plate changer⁴⁾ for SN of steel ladle

band protecting the plate contour. Due to the NQFP and the easy loading and releasing of the contact pressure, it is now possible to open the sliding surface for quick and accurate inspection of the SN plate, which helps to extend the plate service life. **Figure 12** illustrates the NQFP three-dimensionally, and **Fig. 13** shows open inspection of the SN plates.

3.1.4 Compatibility with automatic changer of SN refractories⁴⁾

Krosaki Harima is developing an automatic changer of SN plates using a general-purpose six-axis robot (see **Fig. 14**). To further improve the easy loading and releasing of the contact pressure and good workability of the plate changer of the R Series™, the automatic plate changer is designed to be compatible with the R Series. The automatic plate changer is expected to greatly robotize before long the servicing work for the SNs for steel ladles.

4. Low-temperature-fired, No-impregnation SN Plate, HYPER™

To secure high resistance to heat shocks and corrosion, Al₂O₃-C

material is widely used for the SN plates for steel ladles and tundishes. The SN plates of this material are roughly divided into fired and non-fired plates according to application. Because fired plates tend to be more porous than the non-fired types as a result of the structural change during the heating, they are densified by impregnating with tar, pitch, etc. after the firing.⁵⁾

On the other hand, when the SN plates of Al₂O₃-C are used for steel grades of high oxygen concentration, they wear significantly by oxidation and corrosion.⁶⁾ By adding Al to the Al₂O₃-C plates, the resistance to oxidation and corrosion is improved and they can be used for high-oxygen steels,⁷⁾ but the portion around the nozzle hole is sintered excessively during the casting, the elastic modulus increases, and edge chipping and similar problems are likely to occur. When Al-added SN plates are heated, densified layers are observed near the surface in some cases, but there have been only a few study reports on the relationship between the Al addition amount and the formation of dense surface layers.^{8, 9)}

In consideration of the above, Krosaki Harima has developed HYPER™, a new no-impregnation material for SNs having properties improved through statistic operation. With high Al addition, a dense surface layer is formed in SN plates under the heat during actual use, the wear is suppressed, and performance equal to or better than that of fired and impregnated plates is obtained. This is described below in more detail.

4.1 Development studies

To investigate the effects of Al addition over the formation of densified surface layers on the work-surface side of a SN plate, Al₂O₃-C plate specimens were prepared by adding Al by up to 9 mass%. After firing them at 1 500°C for 3 h, apparent porosity and permeability were measured, the mineral phases were identified by X-ray diffraction, and densified surface layers and reaction progress were observed through a reflecting microscope. Then, the samples were subjected to a test of reaction with molten steel in a high-frequency induction furnace, and the existence or otherwise of densified surface layers was examined at section surfaces.

Figure 15 shows the relationship between the Al addition amount and the formation of mineral phases. Carbides such as Al₄C₃ negligibly formed with Al addition by 3 mass% or less, but when the Al addition exceeded 6 mass%, the formation of Al₄C₃, Al₂OC, and Al₄O₄C increased.

Figure 16 shows the relationship between the Al addition amount, apparent porosity, and permeability. Apparent porosity was found to decrease with the increase in Al addition. This is presumably because metallic Al reacted with oxygen and carbon, and its volume expanded to fill the voids in near-by regions, densifying the internal structure.

On the other hand, permeability is considered to have decreased as a result of densification of the internal structure and the formation of the densified surface layer due to the increase in the Al addition up to 6 mass%.

Figure 17 shows structural photomicrographs of specimen sections near the surface. While no densified surface layers were seen with the samples of Al addition by 0 and 3 mass%, densified layers roughly 10 μm in thickness were found to have formed in those of Al addition by 6 mass% or more. However, no thicker densified layers were found to form when the Al addition was further increased.

Figure 18 shows sectional photomicrographs near the surface of the samples after the test of reaction with molten steel. An oxidation layer was found at the surface of each sample, and its thickness was found to decrease with the increase in Al addition. This layer formed

presumably through the reaction between oxygen in the steel and carbon in the specimens.

4.2 Test of commercial use

Specimens of SN plates for steel ladles were prepared using the material of high Al addition with which the formation of the densified surface layer was confirmed at the test described in the previous sub-section (referred to as material A) and a general-purpose materi-

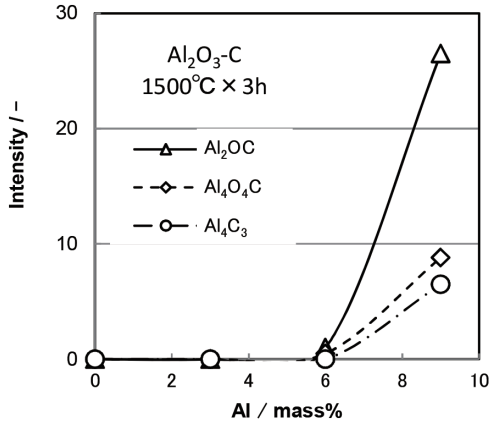


Fig. 15 Relationship between Al addition and X-ray diffraction intensity of mineral phases in Al₂O₃-C refractory

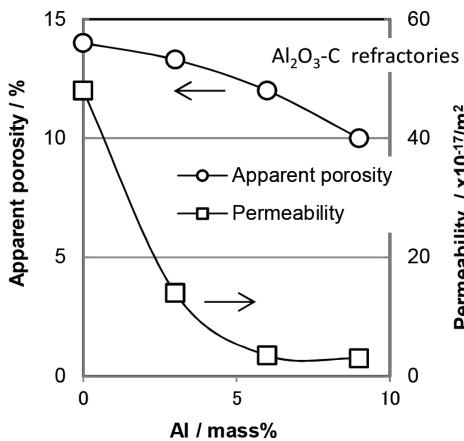


Fig. 16 Relationship between Al mass% and apparent porosity, and permeability on Al₂O₃-C refractories

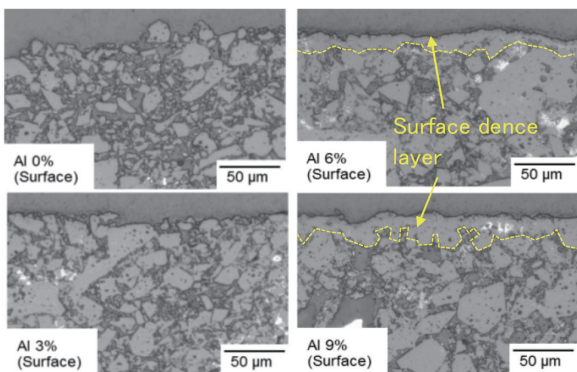


Fig. 17 Microstructure change in the fired Al₂O₃-C refractories with Al addition

al (referred to as material B), and after use for real operation, their chemical and physical properties were examined. Table 1 compares the properties of the specimens; note here that material B was impregnated, but material A was not.

Figure 19 shows photographs of the sliding surface of the upper SN plates of the specimens after use on a steel ladle for two charges, and Fig. 20 structural photomicrographs of the same surfaces. It is clear from these photographs that the surface damage of material A is less than that of material B: oxidation and adhesion/flaking of the

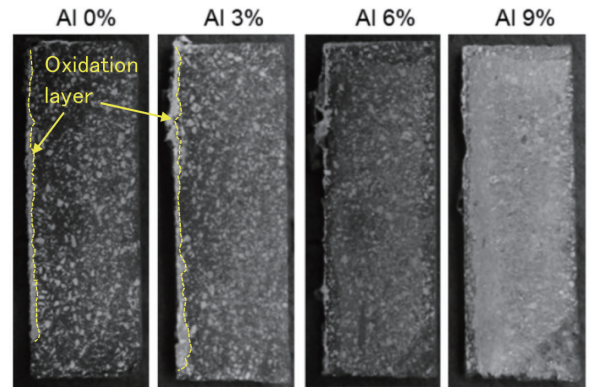


Fig. 18 Cross section of specimens after the molten steel dipping test

Table 1 Properties of materials

Material	A	B
Metal Al content / mass%	2a	a
Chemical composition / mass%	Al ₂ O ₃	93
	ZrO ₂	-
	F.C.	4
Bulk specific gravity / -	2.99	3.28
Apparent porosity / %	14.3	9.0
Bending Strength / MPa	At R.T.	44
	At 1400°C	48
Thermal expansion / %	At 1500°C	1.29

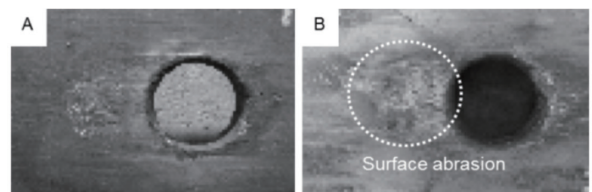


Fig. 19 Surface appearance of SN plates after use: (A) slight roughening, and (B) significant roughening

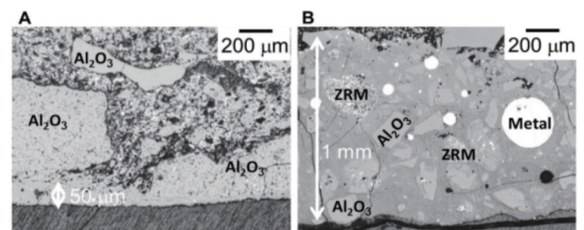


Fig. 20 Comparison of the microstructure of the SN plate after use

latter are pronounced. At structural observation of the two, a densified surface layer roughly 50 μm in thickness was found to have formed at the sliding surface of material A, and a sound structure remained inside. With material B, in contrast, slag-like substance and steel were found to penetrate more than 1 000 μm through the sliding surface layer, and active reactions between the aggregate, the matrix, and the slag-like substance were found to have taken place conspicuously. These findings seem to indicate that, in material A, the added metallic Al formed the densified surface layer to reduce the wear as stated in sub-section 4.1.

5. Submerged Entry Nozzle for Continuous Casting, FANON™-TUBE

5.1 Improvement of heat-shock resistance of alumina-graphite material

High functions such as molten steel transfer, air shutoff, flow control, and elimination of inclusions are required for the entry nozzles for continuous casting, the final process in the steelmaking plant. They are used under very severe environmental conditions. High resistance to heat shock is essential since the temperature of the molten steel flowing through them is 1 500°C or higher. Focusing on reforming the bond (lowering elasticity and raising strength) of the carbon matrix of an alumina-graphite (AG) material, Krosaki Harima has tackled the development of measures to enhance the heat shock resistance of the entry nozzles. Eventually, it has been made possible to improve the heat shock resistance by changing conventional hard and brittle glassy carbon into a crystalline fine carbon structure (hereinafter referred to as FANON™) having comparatively low elasticity. The SENs made of this fine carbon structure having improved heat shock resistance are named FANON™-TUBES.

Figure 21 shows TEM photomicrographs of FANON™ and conventional glassy carbon after firing in a non-oxidizing atmosphere at 1 000°C; a fine carbon structure is seen with FANON™. Table 2 compares the properties of FANON™ that was manufactured by changing only the bond but not changing the grain size distribution and those of a conventional AG material. Although the chemical composition is the same, FANON™ is stronger and less elastic than the other. The table includes the results of a thermal shock resistance test using cylindrical test pieces, conducted as shown in Fig. 22. FANON™ exhibited a significantly better result

than the conventional AG material did. Different from the silica material, the silica grains of which crystallize by heating, the non-silica FANON™ material demonstrates good heat shock resistance. It is expected to contribute to stable casting operation when used for SENs.

5.2 Improvement of wear resistance of zirconia-graphite material¹⁾

SENs tend to wear locally at the powder-line portion¹²⁾ owing to the molten mold powder on the steel surface in the mold, which shortens the nozzle life. For this reason, zirconia-graphite (ZG) material, a mixture of graphite and zirconia, which is excellent in the resistance to the corrosion by the molten powder, is widely used for

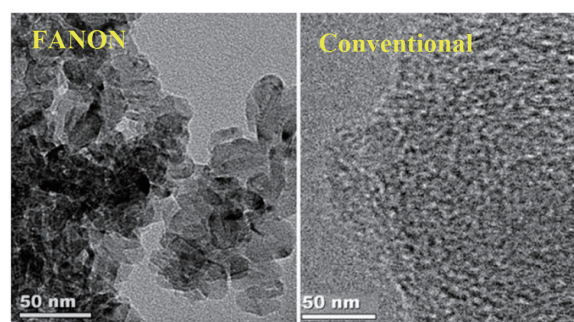


Fig. 21 TEM images of carbon bond after heat treatment

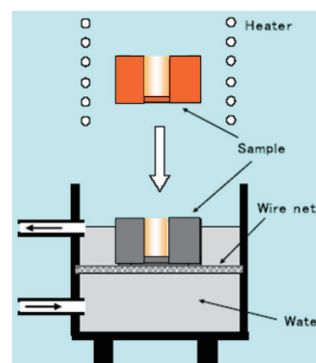


Fig. 22 Thermal shock resistance test by water quenching

Table 2 Comparison of chemical and physical properties of FANON and conventional AG materials

Material	FANON	Conventional	FANON	Conventional	
Silica addition on the material	Non-silica AG		Silica-containing AG		
Chemical composition / mass%	Al ₂ O ₃	68	68	61	61
	F.C.	31	31	25	25
	SiO ₂	—	—	14	14
Tensile strength ¹⁰⁾ S / MPa	5.9	5.0	5.7	4.7	
Hot Bending strength / MPa	At 1 400°C	11.1	10.9	13.9	9.6
Elastic modulus E / GPa		8.0	10.6	9.2	10
Thermal expansion α / %	At 1 000°C	0.4	0.42	0.26	0.28
Thermal shock resistance S · E ⁻¹ · α ⁻¹ / —		1.84	1.12	2.42	1.67
ΔT spalling test results (repeated water quenching from a certain temperature until 10 cycles)	ΔT=1 500°C	○-○-○-○-○	○-×	○-○-○-×	×
	ΔT=1 400°C	○-○-○-○-○	○-○-○-○-○	○-○-○-○-○	×
	ΔT=1 300°C	○-○-○-○-○	○-○-○-○-○	○-○-○-○-○	○-×
	ΔT=1 200°C	○-○-○-○-○	○-○-○-○-○	○-○-○-○-○	○-○-○-×

○: No crack, ×: Crack observed

Table 3 Comparison of properties of FANON and conventional ZG materials

Material	FANON	Conventional	
Chemical composition / mass%	ZrO ₂	86	86
	F.C.	9	9
	CaO	3.7	3.7
Apparent porosity / %	16.2	19.2	
Tensile strength ¹⁰⁾ S / MPa	6.2	4.8	
Hot Bending strength / MPa	At 1400°C	10.5	8.4
Elastic modulus E / GPa	6.1	6.3	
Thermal expansion α / %	At 1000°C	0.33	0.37
Thermal shock resistance S · E ⁻¹ · α ⁻¹ / -	3.08	2.06	
Corrosion index	85	100	

the powder-line portion of SENs. The greater the zirconia content, the higher the corrosion resistance becomes, but when it exceeds 85%, heat shock resistance is lowered and porosity increases, and practically, something around 85% is considered to be the upper limit of the zirconia content. In consideration of the above, we studied the possibility of applying the FANON™ technology to the ZG material containing 86% zirconia having the highest corrosion resistance, without changing the grain size distribution of the raw material. The results are shown in **Table 3** and **Fig. 23**. The same as with the AG material, the structure of the ZG material was densified and strengthened by applying the FANON™ technology. **Figure 24** shows the method of corrosion test for the ZG material. The ZG material modified by the FANON™ technology demonstrated corrosion resistance higher by approximately 15% than that of conventional ZG. In addition, heat shock resistance (ΔT) was improved by 50°C as a result of higher strength and lower elasticity modulus.

6. Closing

As the examples of the recently developed refractory products for the teeming system of continuous casting, the present paper has introduced the clean-flow nozzles, CFN™ and CFP™, designed to stabilize casting operation and improve cast quality, the R Series™ SN units for labor saving of nozzle changing work, the no-impregnation SN plates, HYPER™, a product of the latest studies for functionality enhancement, and the new type of SENs for continuous casting, FANON™-TUBEs. Aiming at higher functionality of the refractory products, we will continue studying and developing refractory products for the steel teeming system of continuous casting

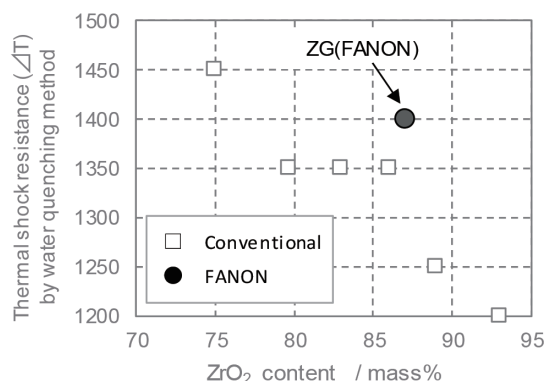


Fig. 23 Comparison of thermal shock resistance (ΔT) between FANON and conventional ZG materials

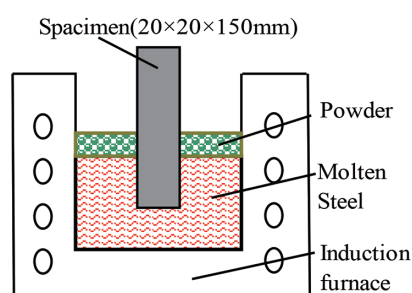


Fig. 24 Powder line corrosion resistance test

to contribute to higher steel quality and productivity.

References

- Ogibayashi, S.: Taikabutsu. 46 (4), 166 (1994)
- Mizobe, A. et al.: Taikabutsu. 63 (2), 65 (2011)
- Mizobe, A. et al.: Taikabutsu. 69 (2), 58 (2017)
- Yoshimura, M. et al.: UNITECR2019, 2019, p.150–153
- Refractories Handbook '97. The Technical Association of Refractories, Japan, 1997, p.122–124
- Sugino, T. et al.: Taikabutsu. 44 (5), 263 (1992)
- Shikano, H. et al.: Taikabutsu. 39 (11), 638 (1987)
- Kawasaki, Y. et al.: Taikabutsu. 59 (3), 122 (2007)
- Makino, T. et al.: Taikabutsu. 66 (3), 139 (2014)
- Japanese Unexamined Patent Application Publication No. H11-64198. March 5, 1999
- Yoshitsugu, D. et al.: UNITECR2007, 2007, p.349–352
- Mukai, K. et al.: Taikabutsu. 41 (11), 646 (1989)



Kentaro IWAMOTO
 Manager
 Flow Control Refractories Division
 Krosaki Harima Corporation
 1-1 Higashihamamachi, Yahatanishi-ku,
 Kitakyushu City, Fukuoka Pref. 806-8586



Toshihiro IMAHASE
 Assistant Manager
 Automation Engineering Group
 Engineering Department
 Krosaki Harima Corporation



Kazuo ITOH
 Director and Chief Production Officer
 SN Refractory Tokai Co.,Ltd.



Kouichi HAREN
 Manager
 Flow Control Refractories Division
 Krosaki Harima Corporation